Conference paper

Rita Del Pezzo, Nuno A.G. Bandeira, Anna Trojanowska, Susana Fernandez Prieto, Todd Underiner, Marta Giamberini and Bartosz Tylkowski*

Ortho-substituted azobenzene: shedding light on new benefits

https://doi.org/10.1515/pac-2018-0719

Abstract: Novel functional polymeric microcapsules, based on modified azobenzene moieties, are exhaustively investigated, both from a theoretical and experimental points of view. Theoretical calculations and several measurements demonstrate that visible light can act as a trigger for release of encapsulated material, as a consequence of *trans-cis* isomerization which modifies microcapsule surface topography and can induce a "squeezing" release mechanism. Interfacial polymerization of an oil-in-water emulsion is performed and leads to core-shell microcapsules which are characterized by means of atomic force microscopy (AFM), optical microscopy (OM), scanning electron microscopy (SEM) and light scattering. These analyses put into evidence that microcapsules' size and surface morphology are strongly affected by irradiation under visible light: moreover, these changes can be reverted by sample exposure to temperatures around 50 °C. This last evidence is also confirmed by NMR kinetic analyses on modified azobenzene moiety. Finally, it is shown that these smart microcapsules can be successfully used to get a controlled release of actives such as fragrancies, as a consequence of visible light irradiation, as confirmed by an olfactive panel.

Keywords: Chemistry for Beauty and Health 2018; interfacial polymerization; microcapsules; ortho-substituted azobenzene.

Introduction

Microencapsulation as a leading interdisciplinary research technology [1] was invented approximately 65 years ago by Green and Schleicher from the National Cash Register Company as a way to encapsulate leuco-dyes for carbonless copy paper. Microcapsules are defined as circular cross-section shaped particles with certain free

Article note: A collection of invited papers based on presentations at the 1st International Conference on Chemistry for Beauty and Health, 13–16 June 2018, Nicolas Copernicus University in Torun, Poland.

***Corresponding author: Bartosz Tylkowski,** Department of Chemical Engineering, Rovira i Virgili University, Av. Països Catalans 26, Tarragona 43007, Spain; Centre Tecnològic de la Química de Catalunya, Carrer Marcelli Domingo s/n, Tarragona 43007, Spain; and The Procter and Gamble Company, 6210 Center Hill Avenue, Cincinnati, OH 45224, USA, e-mail: bartosz.tylkowski@ctqc.org
Rita Del Pezzo: Department of Chemical Engineering, Rovira i Virgili University, Av. Països Catalans 26, Tarragona 43007, Spain; and The Procter and Gamble Company, Temselaan 100, Strombeek-Bever 1853, Belgium
Nuno A.G. Bandeira: Biosystems and Integrative Sciences Institute, Faculty of Sciences, University of Lisbon, Campo Grande-C8, Lisboa 1749-016, Portugal; Centro de Química Estrutural – Instituto Superior Técnico, Universidade de Lisboa, Av. Rovisco Pais, Lisboa 1049-001, Portugal; and Institute of Chemical Research of Catalonia (ICIQ) – Avda. Països Catalans, Tarragona 16-43007, Spain
Anna Trojanowska and Marta Giamberini: Department of Chemical Engineering, Rovira i Virgili University, Av. Països Catalans 26, Tarragona 43007, Spain; and Centre Tecnològic de la Química de Catalunya, Carrer Marcelli Domingo s/n, Tarragona 43007, Spain
Susana Fernandez Prieto: The Procter and Gamble Company, Temselaan 100, Strombeek-Bever 1853, Belgium
Todd Underiner: The Procter and Gamble Company, 6210 Center Hill Avenue, Cincinnati, OH 45224, USA

volume inside in which a core active material can be incorporated [2, 3]. When employed as storage and delivery systems microcapsules gain considerable importance in a number of applications over a broad range of industries including adhesives and coating, dyes and inks, drugs, perfumes, food additives, catalysts, etc. [4–14]. The purpose and challenge of developing an effective delivery system is the controlled release of encapsulated ingredients [15]. During the last decade, several triggers such as: light, temperature, pH change, etc. have been investigated by scientists to boost microcapsule wall morphological changes. These stimuli may introduce some variations in compactness and integrity of capsule walls influencing their shell permeability and in a consequence the release of encapsulated actives [16–18]. Microcapsules based on photo-sensitive moieties open new horizons spanning both industry and academic research [19] due to their numerous benefits over other external stimuli: (a) duration and localization of excitation can be easily controlled, (b) photons do not contaminate the reaction environment, and (c) the excitation wavelength can be tuned through appropriate molecular design [20, 21]. In cases, where light would be the only accessible stimulus to drive the systems, i.e. environmental application, drug release in precise medical delivery systems or surface science, the development of photo-triggered capsules could be highly appreciated [22]. Generation of photo-responsive behavior in microcapsule wall by integration of light sensitive polymers, functional dyes and metal nanoparticles has been described in literature [23]. Azobenzene is one of the most recognized and investigated chromophores in literature [24, 25]. For the first time it was described in 1834 by Prof. Mitscherlich [26]; however pioneer studies concerning a functional optical behavior of azobenzene, based on reversible *trans-cis* isomerization of the N=N bond upon UV-irradiation, were reported by Prof. Hartley in 1937 [27, 28]. Since then this photochromic moiety has been broadly applied in the design of light-triggered materials [29], thus various approaches have been performed to develop azobenzene-based photo-sensitive capsules with diverse functionalities [30–38].

The *trans-cis* photo-isomerization process can occur via two routes: excitation to a symmetry forbidden n-π* state (S_1) that shows up in the visible region (formally symmetry forbidden) or excitation of the system in the near-UV region to a π-π* state (S_2) revealing a large absorption intensity. Interestingly the quantum yield of the interconversion [39] in azobenzene is higher in S_1 (~0.3) than it is for S_2 (~0.2).

Several groups have reported computational works concerning the photochemical and spectral properties of azobenzene [40–46] where attempts have been made to resolve the long running debate over which reaction coordinate pathway is followed – the dihedral torsion ∡(CNNC) or the twisting of one of the rings ∡(NNC). The latest work by Casellas and co-workers [47] is the most comprehensive work yet on the dynamics of the several excited states in azobenzene. The main outcomes from the global potential energy landscape were that excitation to the S_1 state goes through the rotational mechanism whereas through S_2 the pathway is bifurcated between rotation and a restricted pedal like motion. Upon pursuing the latter route the system may revert back to the *trans* isomer which explains the lower quantum yield of S_2.

Recently, Beharry et al. [20] demonstrated that ortho-substitution of a methoxy-group in the azo moiety can significantly red-shift the n-π* band wavelength while blue-shifting the π-π* band. This behavior is in line with what is known from classic studies regarding ortho- and para- substituents [48, 49]. Other important factors affecting the photo-isomerization kinetics are also the solvent polarity [50]. Woolley and co-workers [51] reported that ortho-substituted azobenzene cross-linkers could be photo-isomerized with red light ($\lambda = 635$ nm), while Aprahamian and co-workers [52] and Hecht and co-workers [53] have demonstrated that BF_2-coordinated azobenzenes and ortho-fluoro-substituted azobenzenes, respectively, possess visible light switching properties.

According to literature, the mobility and stability of the azobenzene moieties in a polymer film are strongly influenced by the length and the rigidity of the spacer connecting them [54]. It has been reported that, when the flexible spacer is sufficiently long, such as 6–8 methylene units, spacer length does not significantly impact the alignment of the azobenzene group. However, when the spacer contains fewer than six methylene units, it is too short to allow for sufficient motion. Moreover, Irie and Suzuki [55] reported that, when the azobenzene moieties in the main chain of the polymer are connected only by flexible spacers, the azobenzene configurational isomerization could scarcely affect the polymer's overall conformation.

In the present work, we explored the potential application of polymeric microcapsules based on modified azobenzene moieties, which can effectively release their content under the simple action of visible light.

Furthermore, we performed a computational investigation of the two main electronic transitions and how these affect the structural distortion of the photo-agent during the interconversion process, to elucidate the photo-physical and chemical properties of the azo-polymer.

The polymeric microcapsule shell was designed and fabricated by interfacial polymerization method and the resulting microcapsules were characterized. Moreover, we demonstrated that this novel advanced material can successfully control the release of, for instance, fragrancies, through visible light triggering, as confirmed by an olfactive panel.

Results and discussion

Computational studies

A considerable number of computational studies have been devoted to the un-substituted azobenzene molecule with regards to its photoisomerization [56–58]. Herein, we present a computational characterization of the monomeric unit of ortho-substituted azobenzene to elucidate its structural features in the microcapsules. The dynamics of the photochemical and thermal processes are analyzed by a potential energy surface analysis and the calculation of the transition states (TSs) following both the inversion and rotation reaction coordinates using spin flip TDDFT methodology.

First, we performed a computational analysis taking as a model 4,4′-(diazene-1,2-diyl)bis(3-methoxy-N-methylbenzamide) (**A**) since it is the leading photoactive moiety in the interconversion process. The *cis*-**A** and *trans*-**A** forms have C_2 and C_{2h} point group symmetries, respectively. As expected the optimized minima clearly show that there is a disparity in the chain lengths of each structure. This can be measured approximately by the distance between the distal carbons in each isomer. *Trans*-**A** has 16.8 Å whereas *cis*-**A** 10.1 Å (Fig. 1a).

As referred previously the principal electronic transitions from azobenzene derivatives involved in the photo-excitation process observed in the UV-Vis absorption spectrum are known to be n→π* (S_1, symmetry forbidden) appearing in the visible region and π→π* (S_2, symmetry allowed) transition appearing in the

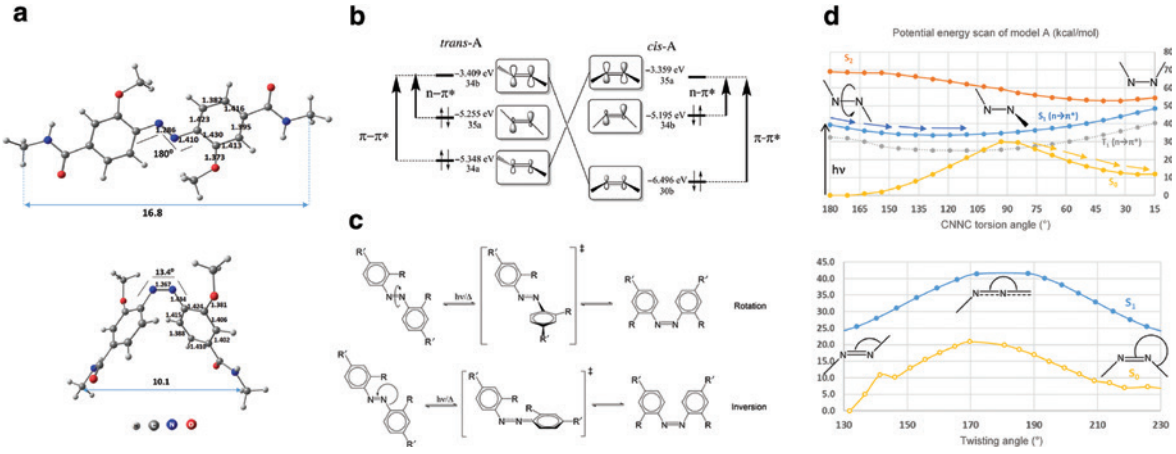

Fig. 1: (a) BLYP optimized structures of *trans*- (above) and *cis*-(below) 4,4′-(diazene-1,2-diyl)bis(3-methoxy-N-methylbenzamide) with relevant structural parameters (Å, degrees); (b) Kohn-Sham orbital energies (C_2 point group symmetry) and molecular orbital correspondence between both stereo-isomers; (c) possible mechanisms for thermal and photochemical isomerisation of *trans* to *cis* azobenzene derivatives with substituents in the ortho- and para-positions relative to the azo-functional group; (d) potential energy surface scan as a function of the ∠CNNC dihedral (above) and ∠NNC angle (below) for the S_0 and S_1 states. The kink in the S_0 curve at 143° is due to a structural change in the plane of the aryl ring when it is more favorable for it to be perpendicular relative to the azo-group.

near- to ultraviolet region. The letter n indicates the nitrogen lone pairs and π and π* are the in and out of phase linear combination of 2p orbitals perpendicular to the bond axis. For model **A** the calculated HOMO-LUMO gaps are larger by 10 meV for the *trans*- isomer than for the *cis*- structure, a similar trend also is present in azobenzene (Fig. 1b).

The photo-induced inter-conversion has long been a subject of debate since unlike stilbene which does not have lone pairs the conversion process may undergo both excitation pathways (S_1 and S_2). Since the n→π* excited molecule has an overall π bond order of ½ it was previously assumed that this isomerisation pathway did not undergo a rotation of the aryl planes, the –CNNC– torsion, but rather an inversion or twisting of the –NNC– angle, passing through a sp hybridized transition state (TS) in the process (Fig. 1c). However, since the works of Cembran and Gagliardi [42, 43] it has been known that the most important reaction coordinate of the S_1 pathway is the aryl plane torsion and may involve a not insignificant inter-system crossing between the ground state (S_0) and triplet (T_1) potential energy seams. The ground state (S_0) and S_1 potential energy curves are able to intersect as they belong to different point group symmetries at a ∠(CNNC) angle of about 90°. This means that a vibrational relaxation can allow the molecule to transition from one surface to another.

To gain a better insight into the energy requirements and structural transformations that both mechanisms require for model A, we performed a reaction coordinate potential energy surface (PES) scan on both the ground and first excited states, considering both mechanisms presented in Fig. 1c. The geometries were optimized using the response density of the ground state triplet (T_1) ground state using the time dependent spin flip procedure (SF-TDDFT) to circumvent any static correlation problems (see Computational details). The photochemical excitation of S_0 to S_1 allows for an easy ∠(CNNC) dihedral angle rotation as the S_1 potential energy surface is quite shallow (Fig. 1d) on the basis of the weaker π bond, allowing the system to relax into the *cis*-**A** form. The S_2 surface is shaped as a reversed 'S' and goes downhill from the *trans*- geometry into a minimum at approximately ∠(CNNC) = 45° from which point it will decay radiatively. At ∠(CNNC) = 90° there is a conical intersection from the S_1 surface to S_0 and the system undergoes a non-radiative decay to the *cis* form. In addition the electron may also make a transition radiatively from S_2 to the S_1 curve, cross over to S_0 and thermally relax either to the *cis* or *trans* isomers.

This PES scan is similar to the ones reported previously for azobenzene [43, 47], and to one calculated for *o*-azophenol by Steinwand and others [59].

Considering the ∠(NNC) angle twisting or inversion mechanism it may be seen from the PES that the straightforward photochemical process is not possible via the S_1 surface since, like S_0, it requires thermal activation. Pursuing the ∠(NNC) reaction coordinate through the S_1 curve causes the ∠(CNNC) dihedral to loosen making it less clear for the geometries in each point of the PES to be associated with a *cis* or *trans* conformation. The vibrational mode of this dihedral is too floppy. The stereochemistry of this change is sketched in Fig. 2a.

This is consistent with the findings of Cembran and others [42] whereupon the twisting coordinate may play a role but only if it is associated with the dihedral rotation coordinate at some point during the isomer switching reaction so as to become energetically viable. It is thus absurd to consider the ∠NNC coordinate independently. The thermal inter-conversion rate is known to be largely insensitive to the electronic nature of para- substituents [48, 50]. For this reason the calculated PES in Fig. 1d is not dissimilar to that of azobenzene. The electronic structure of the torsional transition state with the lowest energy is as expected the triplet (T_1) since it is the lowest energy root when ∠(CNNC) is in the 90° region (Fig. 1d).

Both of the highest points in the two S_0 states of PES (a) and (b) were re-optimized (the first spin flip root from the corresponding the triplet density) so as to obtain a more quantitative assessment of the thermal barriers for both mechanisms.

For model **A** the structural features of these TS's are depicted in Fig. 1b. The S_0 minima *cis*- and *trans*-**A** each underwent a TDDFT single point calculation to obtain the corresponding transition frequencies. A summary of these optical properties and thermal conversion barriers of **A** are presented in Table 1.

It can be seen that absorption intensities of the *trans*- isomer are larger in the visible region as expected since this transition is allowed by symmetry. The n-π* transition energy is symmetry forbidden for this isomer and as such its oscillator strength is strictly zero. This weak shoulder usually comes up in the visible region due to structural deviations from C_{2h} symmetry.

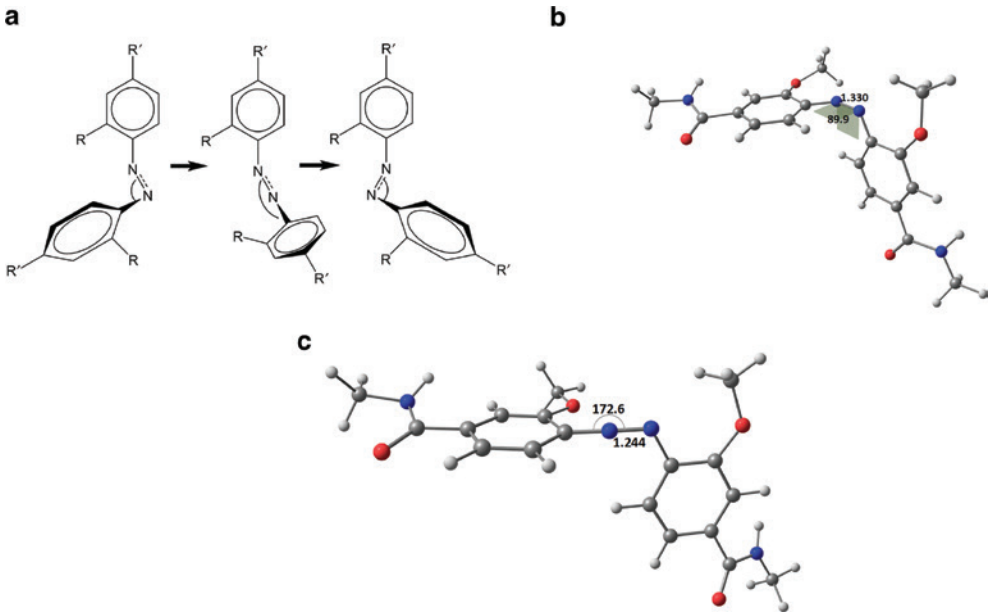

Fig. 2: (a) ∠(NNC) reaction coordinate in PES; (b) transition state structures belonging to the rotation and inversion (c) pathways of model A (distances in Å, angles in degrees).

Table 1: Calculated TD-BLYP vertical electronic transition energies of model **A** (left) and potential energy barrier heights ($\Delta E^{\ddagger}$/kcal · mol^{-1}) for thermal interconversion in the S_0 state.

Isomer	E (n-π^*)/nm	f(OS)	E (π-π^*)/nm	f(OS)	Inversion barrier ($\Delta E^{\ddagger}$/kcal · mol^{-1})	Rotational barrier ($\Delta E^{\ddagger}$/kcal · mol^{-1})
trans-**A**	608	0	494	0.376	+26.5	+33.0
cis-*A*	561	0.113	365	0.102		

The energies of the thermal interconversions show a remarkable opposite trend to what is expected in that the inversion barrier is energetically preferred over the rotational one. There might well be other instances where substituent effects may play a role in stabilizing one TS over another. In any case the photochemical activation is thermally more favorable through the rotation mechanism (whether through S_1 or S_2) whereas the inversion mechanism always requires a greater vibrational stimulus in the form of heat to operate.

Experimental studies

The design of the new photo-sensitive microcapsule shell, synthesized by interfacial polycondensation of an oil-in-water dispersion, is illustrated in Fig. 3. Figure 4a shows the results of optical microscopy (OM) of the polyamide microcapsules, containing PC1025-2 perfume oil, after their preparation. Figure 4b shows the cross-section morphology captured by cryo scanning electron microscopy (Cryo-SEM). The microcapsules appear well formed and globe-shaped with a dense wall. The main size diameter of the capsules (62.2 ± 0.3 μm) was measured by the light scattering (LS) method; 90 % of the capsule diameters were in the range 20–85 μm. This range is comparable with the size of polyamide microcapsules prepared by interfacial polymerization reported in literature [60]. Wall thickness was measured by Image-ProPlus 5 software (Media Cybernetics Inc., Rockville, MD, USA) from cross-section SEM micrographs and gave a value 49 ± 3 nm. GC-MS analysis of free perfume in microcapsules suspension, developed by Smets [61], put into evidence that by using the interfacial polymerization method 99.51 % ± 0.09 % of perfume oil was encapsulated.

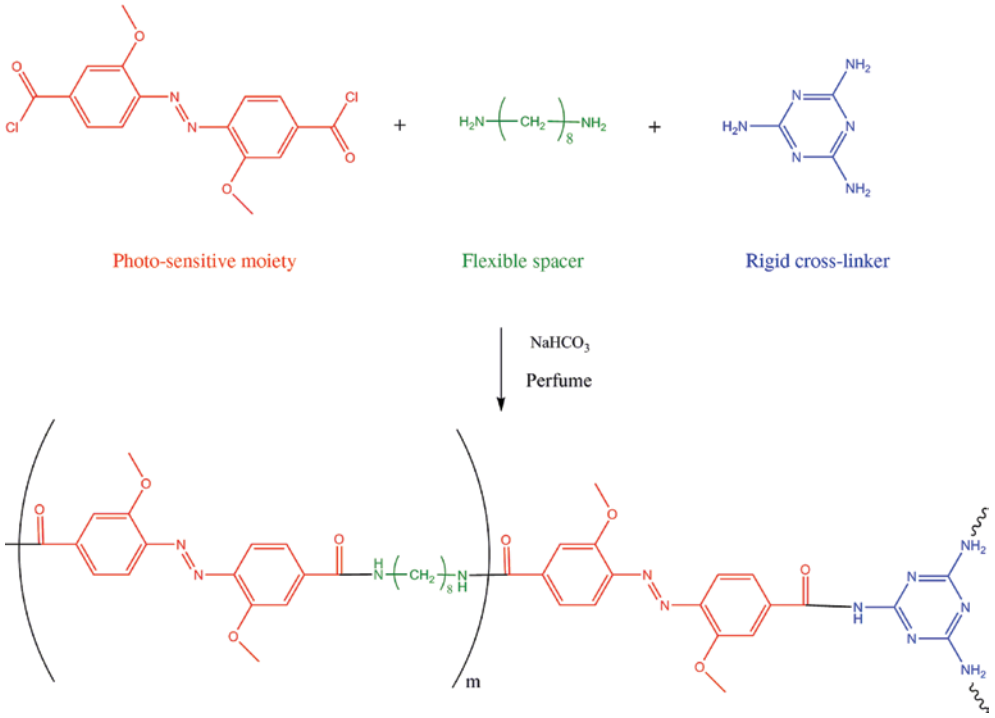

Fig. 3: Formation of microcapsule wall.

In order to evaluate the effect of visible light irradiation on the microcapsules' morphology, the microcapsules were exposed to visible light emitted from a microscopy bulb for up to 1 h and then kept in darkness overnight. Figure 4c shows how a single microcapsule's shape is changing as a function of time and light exposure. During the first 6 min of irradiation the microcapsule seems to be well formed with a smooth surface. Then, after additional 3 min of irradiation its surface morphology starts to change and the microcapsule's diameter decreases approximately 7 %. After an elapsed 12 min of irradiation the diameter decreases by 11 % from the initial, and its surface appears rough. No further morphological changes were observed after 12 min to 1 h of additional irradiation. During the next step the capsule was kept in a light deprived environment for 15 h and its morphology was again observed. As it is shown in Fig. 4c, its surface has turned back to well defined and spherical, like at the beginning of the experiment. Further, the capsule's diameter after resting in darkness is now only 2 % smaller than the starting capsule prior to irradiation. To confirm these diameter changes, caused by light, additional experiments were performed. From an aqueous dispersion of microcapsules, mean diameter measurements were taken by light scattering prior to and after 1 h of light exposure to visible light emitted by a desk lamp equipped with a Philips DuraMax 85W 120V bulb. The measurement was taken again after 15 h in a dark environment. The mean diameter was found to be 62.23 ± 0.03, 49.46 ± 0.02, and 54.11 ± 0.03 µm, respectively. This corresponds to a 21 % reduction in mean diameter after 1 h of irradiation, and a recovery to 87 % of the original diameter after 15 h in the dark in broad agreement with the microscopy results on a single capsule. Then, in order to understand the microcapsule surface topography change occurring during irradiation with visible light, additional computational studies using a BIOVIA Materials studio (Accelrys) platform were performed. By using the Polymer Builder module we created surface models containing five chains of polyamide formed by the five ortho-substituted azobenzene moieties connected by 1,8-diamminooctane, as flexible spacers. Figure 4d visualizes the *trans* and *cis* topographies of these surfaces. While the *trans* topography is greatly symmetrical exhibiting a planarity, the *cis* topography is much more geometrically irregular and approximately 20 ± 1 % shorter than the one formed by the *trans*-polymers. This simulation suggests that the *trans-cis* photo-isomerization of the ortho-substituted azobenzene moieties incorporated in the main chain of the polymer which forms microcapsule shell, leads to the capsule squeezing and consequent release of encapsulated active materials. Furthermore, to understand the morphology changes and the behavior of the

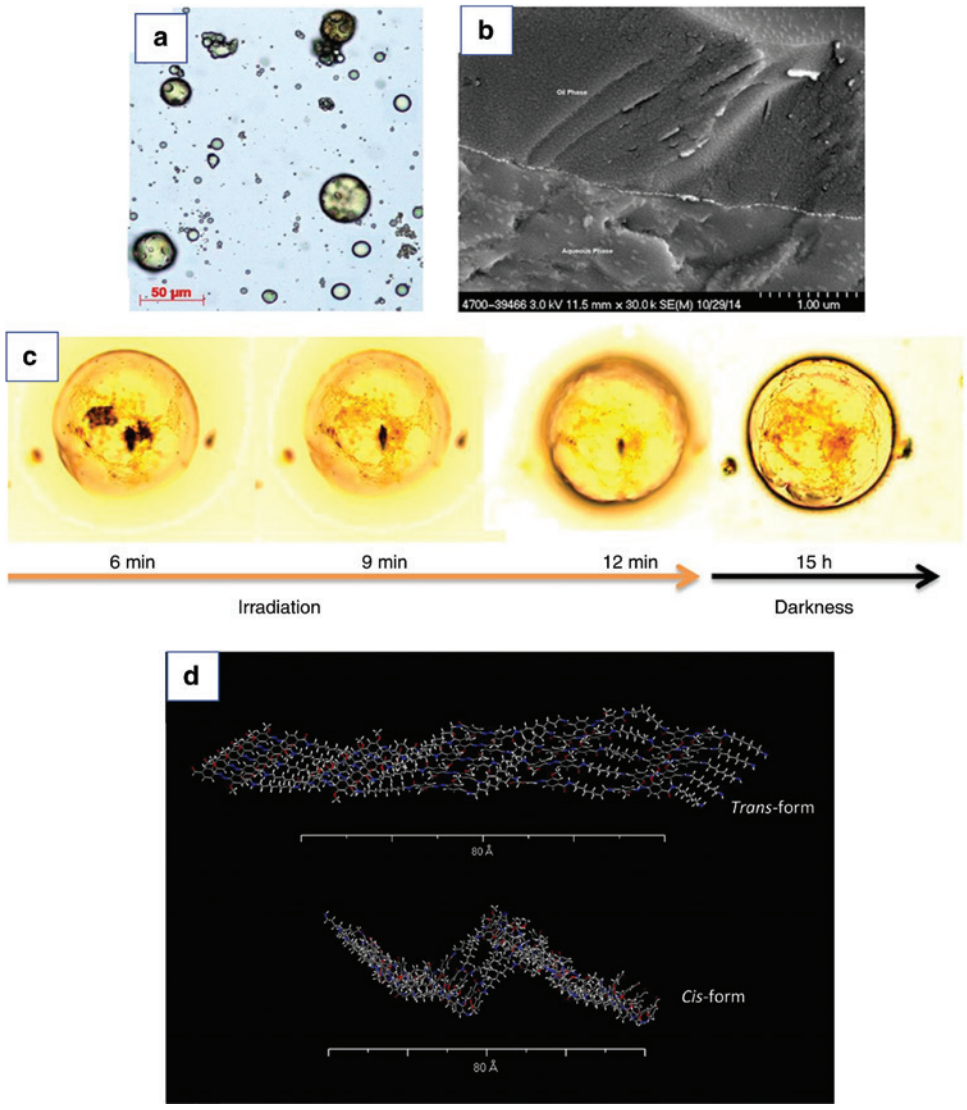

Fig. 4: (a) Optical micrograph of the capsules after preparation; (b) SEM micrograph of the microcapsules cross-section; (c) optical micrographs of microcapsule morphology changing during irradiation with visible light emitted from a microscopy bulb; (d) *trans* (a) and *cis* (b) structures of azobenzene polymer forming microcapsule shell.

microcapsule shell during irradiation, an exhaustive characterization of the microcapsule surfaces was performed by atomic force microscopy (AFM). As it is shown in Fig. 5a, in order to follow the microcapsule's surface topography changes, specific features in the AFM topographies were analyzed by line profiling routines. Linear scans (x direction) and topographic analyzes (z direction) were investigated between two points forming profile 1 and profile 2, at the beginning of the experiments, as well as after 10 and 35 min of irradiation, respectively. As, it can be observed in Cycle I of Fig. 5a, during the first 10 min of light irradiation the *trans-cis* photoisomerization occurs causing the topographic changes. Then a prolonged illumination (11–35 min) causes an unexpected shape change of profiles 1 and 2. They are similar to those measured before sample irradiation. These results suggest a back *cis-trans* isomerization, which according to literature can be driven by sample heating [62, 63]. For this reason, the temperature of the microcapsule surface during the AFM investigation was monitored by Omega MDSi8 thermometer equipped with a thermocouple. Obtained results put into evidence that the bulb emits heat, and increases the sample temperature from 22±2 °C up to 50±2 °C after approximately 25 min of irradiation: this thermal effect could be responsible of the observed topographic variation. Therefore, to prove a cyclic on-off switching effect of photo/thermal isomerizations, the sample surface, initially at room

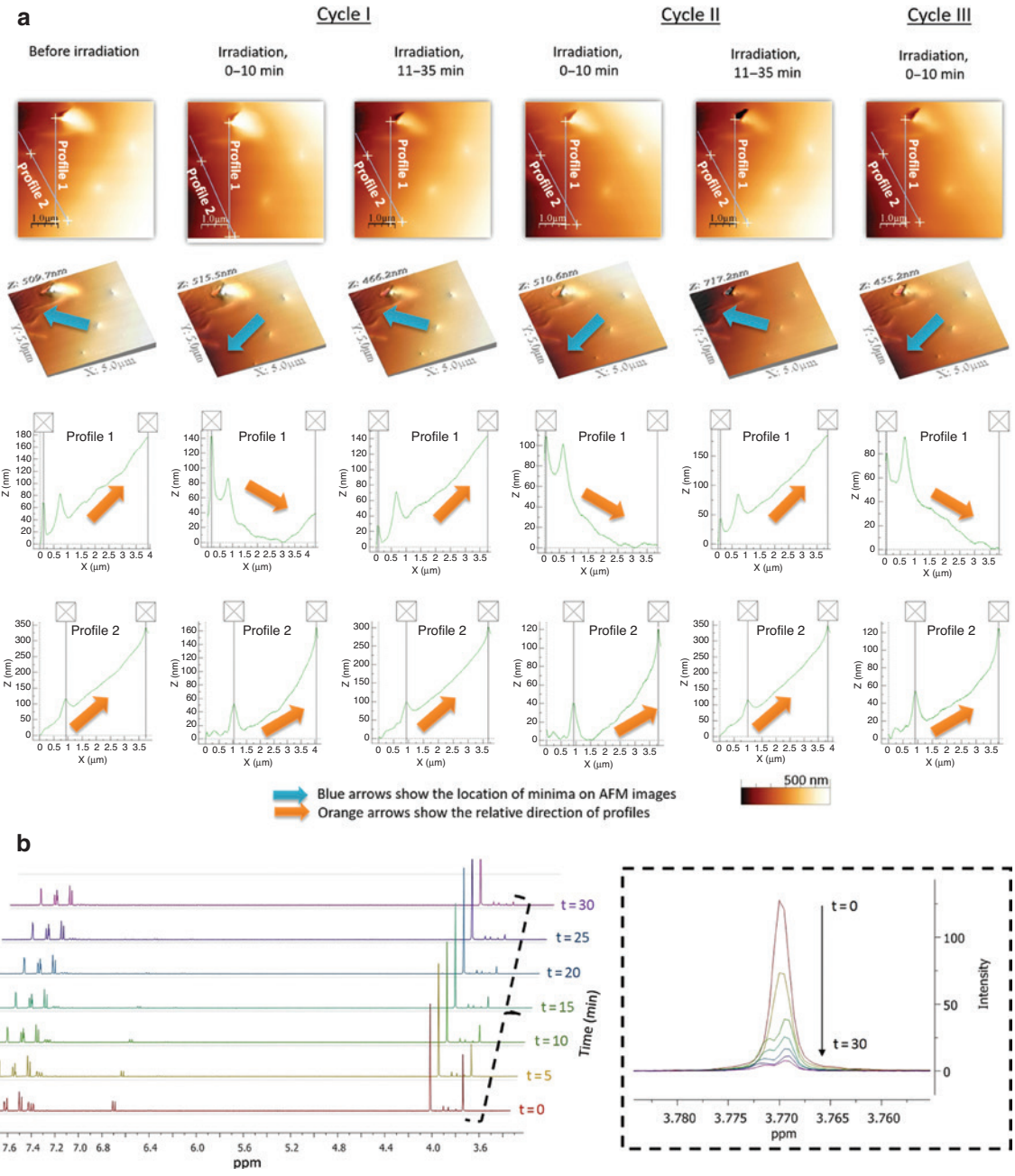

Fig. 5: (a) AFM topographies of microcapsule surface changes caused by visible light irradiation; (b) kinetic of thermal back isomerization at 70 °C starting from a mixture of *trans* and *cis* isomers.

temperature, was submitted to cycles of photo-irradiation/heating to 50 °C and its topographies recorded after each step (Fig. 5a Cycle II and III). AFM experiments clearly confirmed that the topographic changes depend on *trans-cis* photoisomerization, followed by thermal back-isomerization. Further insight of this phenomenon was given by ^{1}H-NMR analysis of the photo-sensitive monomer azobenzene-2,2′-dimethoxy-4,4′-dicarboxylic acid in deuterated dimethyl sulfoxide (d-DMSO). Starting from a mixture of *cis* and *trans* isomers, obtained through irradiation of the sample for 30 min by sunlight, the azo compound was heated into the NMR spectrometer and kept at fixed temperature for 30 min. The spectra were recorded every 5 min to monitor how the concentration of the two isomers in the mixture changed. The described procedure was repeated at four different temperatures, namely 30, 50, 60, and 70 °C (±2 °C) for the study of the thermal back isomerization. At room temperature (20 ± 2 °C), the comparison of the areas of the peaks at 4.05 ppm and 3.77 ppm, which corresponds to the protons

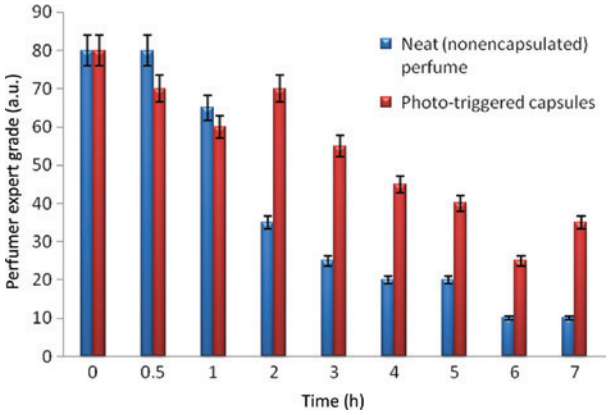

Fig. 6: Comparison of perfume release noticability from fabric under visible light irradiation over time, evaluated by perfumer panelist experts.

of the methoxy group in the *trans* and *cis* configuration, respectively, shows that after 30 min of sunlight exposure the azobenzene-2,2′-dimethoxy-4,4′-dicarboxylic acid is 50 % in its *cis* form. As expected, the thermal back relaxation at 30° is very slow and after 30 min only the 2.4 % of the *cis* isomer in the starting mixture has reverted to *trans*. However, the kinetics at higher temperatures is much more representative of the thermic process: as a matter of example, Fig. 5b shows the ^{1}H-NMR spectrum in d-DMSO of azobenzene-2,2′-dimethoxy-4,4′-dicarboxylic acid recorded in darkness at 70 °C at different times comprised between t = 0 (soon afterwards 30 min sun exposure) and t = 30 min. The inset shows the magnification of the peak at 3.77 ppm which corresponds to the methoxy group of the *cis* ortho-substituted azobenzene and which was selected as a reference to study the kinetic of thermal back isomerization. At this temperature, higher speed of isomerization was found and, after 30 min of heating, only approximately 9 % of the *cis* isomer remained in the studied mixture. Moreover, the experimental data of the thermal back isomerization were analyzed considering a first order kinetic for the isomerization process [64], as showed in the Experimental section. The values for the kinetic constants in d-DMSO ranged between 1.3×10^{-3} and 1.0×10^{-5} s^{-1} recorded at 70 and 30 °C, respectively, which are in agreement with literature findings [20]. In addition, the activation energy of the thermal back isomerization was calculated (see the Experimental section) and exhibited a value of 105.6 kJ/mol, that is comparable with other values reported in literature [64, 65]. Summing up, the whole set of AFM and ^{1}H-NMR experiments suggests the intriguing possibility of a reversible switching of active compounds release from microcapsules upon combination of visible light and thermal stimuli. In order to demonstrate a consumer relevant benefit of photo-sensitive microcapsules application in consumer goods, we performed a sensory evaluation with perfume experts, according to standard tests reported in the literature [66]. The grading scale utilized by perfume experts is adapted to consumer noticeability: a grade less than 20 is not considered as consumer noticeable in this test. During this test based on the trained panelists' nose, we compared the release of the perfume from fabrics exposed to daytime light over time. At the beginning of the test, the fabrics were treated with prototypes containing encapsulated or neat perfume. As shown in Fig. 6, the encapsulated perfume perception over time shows a significant difference, versus the neat perfume one, which is clearly related to a difference in release. The preliminary results clearly demonstrate that the encapsulated perfume shows delayed release and is noticeable up to 7 h, while the nonencapsulated perfume is not detected by the standard consumer after 3 h.

Conclusions

In this work we showed that by incorporating 4,4′-bis(chlorocarbonyl)-2,2′-dimethoxy azobenzene (ortho-substituted azobenzene) moieties into polyamide microcapsule shells, it is possible to trigger active components release by simple exposure to visible light. This is due to light-driven *trans-cis* isomerization which modifies shell morphology, as it was first predicted by computational studies and subsequently confirmed by experimental

preparation of the photoactive polymeric material. By using interfacial polymerization, we succeeded in encapsulating more than 99 % of active agent in globular shaped and separated, well-formed microcapsules. OM and AFM analyses confirmed that photoirradiation induces a change in capsules surface and morphology, as well as size. Both theoretical and experimental studies suggest that a squeezing effect can be responsible for photo-triggered increased release. Moreover, the combination of AFM and ^{1}H-NMR put into evidence that the pristine morphology and size are restored as a consequence of thermal back-isomerization above 50 °C.

Two models of the polymer were computationally analyzed with regards to isomer conversion pursued in the lowest excited states S_0–S_2. The photo-excitation process through the visible light pathway (S_1) changes the dihedral angle ∡(CNNC) and through thermal relaxation reaches a conical intersection with the S_0 surface at an intermediate angle, and decays non-radiatively onto the *cis-* isomer. While the rotation mechanism is the most favorable one photochemically, the thermal barrier for the inversion mechanism is more favorable (26.5 kcal/mol) thus accounting for the heat reliance of the *cis-trans* reconversion. As the cis- isomer is thermodynamically less stable the kinetic barrier can be surpassed by heating the polymer causing it to change to the more stable *trans* form.

Finally, experts' test adapted to consumers and based on perfume perception, showed that after 7 h the encapsulated perfume can be still noticed, while the neat one is not perceived after 3 h. In view of the generated results, the obtained microcapsules can have future potential applications in: consumer goods (household and personal care products), medicine, catalysis, electronics, textile, chemical industry, and others.

Experimental section

Materials

1,8-Diaminooctane (Fluka, 98 %), melamine (Sigma-Aldrich, 99 %), sodium hydrogenocarbonate (Aldrich, 99.7 %), Mowiol (polyvinyl alcohol 18-88, Fluka), 3-methoxy-4-nitrobenzoic acid (Sigma-Aldrich, 99), d-(+)-glucose (Sigma, 99.5 %), sodium hydroxide (Sigma-Aldrich), glacial acetic acid (Sigma-Algrich, 99.5 %), triethylamine (Sigma-Aldrich, 99 %), and thionyl chloride (Sigma-Aldrich, 97 %) were used as received without any further purification. PC1025-2 perfume oil, with a composition described in the US patent application 20130039962, was provided by Procter & Gamble Company. All the solvents were supplied by Scharlau and used without previous purification as received.

Computational details

The Amsterdam density functional (ADF) program package [67, 68] version 2014.10 has been used with Becke's [69] gradient corrected exchange and Lee et al.'s correlation [70] functionals (BLYP) were used in the calculations. The triple zeta Slater type orbital [71] (STO) basis sets augmented with one polarization function (TZP) were used throughout except the potential energy surface scans in which a smaller double-zeta (DZP) basis set was employed for expediency. The time-dependent DFT formalism [72] within the Tamm-Dancoff approximation and in its spin-flip variant (SF-TDDFT) was employed to optimize transition states (TSs) and extract the energy barriers circumventing the multi-reference problem. The dihedral rotation transition state calculations had C_2 point symmetry constraints and none were present (C_1) in the calculation of the inversion TS's. The reference state to obtain the latter was the T_1 ($n^1\pi^{*1}$) triplet. The energies of the corresponding *trans-* isomer resting states were optimized using a conventional static approach (single reference ground state S_0). Calculation of transition wavelengths and intensities were carried out via single points on the previously optimized structures with a 60 root CI window.

In all the time-dependent calculations the T_1 triplet was the reference state from which the response density was calculated. The $m_s = 0$ component of the triplet state (T_1) and the open shell singlet (S_1) can be

differentiated by examining the phase of the CI expansion present in the formatted TAPE21 file. All (SF-) TDDFT gradients were calculated using a 10 root selection of the corresponding symmetry sub-species of the target state.

The Materials Studio program suite was used to create the bulk polymer in periodic boundary conditions starting off from the coordinates of the molecular models. The unit cell was then optimized by deploying the VAMP module [73] using the Parametric Model 3 (PM3) semi-empirical method by Stewart [74].

Synthesis of 4,4′-bis(chlorocarbonyl)-2,2′-dimethoxy azobenzene

The photo-sensitive monomer 4,4′-bis(chlorocarbonyl)-2,2′-dimethoxy azobenzene was synthesized in a two-steps procedure, which first involved the synthesis of azobenzene-2,2′-dimethoxy-4,4′-dicarboxylic acid and its subsequent conversion into the acylic chloride. In a typical experiment, 3.55 g (18.00 mmol) of 3-methoxy-4-nitrobenzoic acid and 10 g (25 mmol) of NaOH were mixed in 60 mL of water and heated until the solid dissolved. Then, a hot aqueous glucose solution (20 g of glucose in 30 mL water) was slowly added at 80 °C. A stream of air was passed into the mixture for 48 h. Then the solution was diluted with 200 mL millQ water and acidified with 25 mL acetic acid, thus yielding ortho-substituted azobenzene-4,4′-dicarboxylic acid as a light pink precipitate. This was filtered, washed with 900 mL of distilled water and dried in oven at 80 °C. Yield: 49 %. ^{1}H-NMR (d-DMSO, TMS, d ppm): 4.05 (s, 3H,); 7.50 (dd 12 Hz, 1H); 7.62 (dd 12, 2 Hz, 1H); 7.74 (d, 2 Hz, 1H). In order to get 4,4′-bis(chlorocarbonyl)-2,2′-dimethoxy azobenzene, 4 g (10.93 mmol) of ortho-subsituted azodibenzoic acid was mixed with 15 mL of thionyl chloride and 0.2 mL of triethylamine. The mixture was heated on an oil bath up to 60 °C. Then, the solution was stirred for overnight at room temperature. Unreacted thionyl chloride was removed under reduced pressure and the residue was washed with dry n-hexane (100 mL) and dried under vacuum. Yield: 92 %. ^{1}H-NMR (d-$CDCl_3$, TMS, d ppm): 4.02 (s, 3H) 7.50 (dd 12 Hz, 2H) 7.60 (dd 12, 2 Hz, 2H) 7.68 (d 2 Hz, 1H). The ^{1}H-NMR spectra were recorded with a Varian Gemini 400 MHz spectrometer equipped with a heating chamber. The behavior of ortho-substituted azobenzene in solution at 30, 50, 60, and 70 °C was also studied through ^{1}H-NMR spectroscopy, using deuterated dimethyl sulfoxide (d-DMSO) as solvent and assuming the isomerization process to have a first order kinetic (eq. 1):

$$v = -k[A] \tag{1}$$

where v is the *cis-trans* isomerization rate at each temperature, k is the rate constant and A is the area of the NMR peak selected as reference for the calculation; it represents the concentration of a specific proton in the selected isomer. The same proton in the two isomers, *cis* and *trans*, shows the signals at different ppms. As reference peak the one at 3.77 ppm corresponding to the methoxy group of the *cis* ortho-substituted azobenzene has been selected to study the kinetic of thermal back isomerization and to calculate the activation energy of the thermal relaxation. The activation energy was determined by measuring the temperature dependence of the slope k and fitting the data with the Arrhenius eq. 2:

$$k = A \cdot e^{-\frac{E_a}{RT}} \tag{2}$$

where E_a is the activation energy of the thermal process, R is the universal gas constant, k is the constant rate at each temperature T expressed in Kelvin.

Photo-sensitive microcapsules preparation

The photo-sensitive microcapsules were prepared by using a modified protocol of oil-in-water interfacial polymerization method developed and reported in our previous studies [27]. According to this protocol, first the oil phase was prepared dissolving 0.600 g of 4,4-bis(chlorocarbonyl) azobenzene in 25 mL of PC1025-2 perfume oil.

Then, to get an oil-in-water emulsion, the oil phase was slowly added drop wise into 50 mL of aqueous solution containing 0.500 g of Mowiol emulsifier (10 g/L) under an overhead stirrer set up at 1200 rpm. Obtained emulsion was additionally mixed for 10 min at room temperature. To obtain the capsules shell, the interfacial polymerization was initiated by adding to the system 25 mL of aqueous solution containing 0.250 g of 1,8-diaminooctane, 0.290 g of sodium hydrogen carbonate, 0.032 g of melamine and 0.250 g of Mowiol. The reaction was carried out in darkness at room temperature for 3 h. Finally, it was stopped by addition of 50.00 g of aqueous solution containing 6.00 g of sodium sulfate and 0.35 g of xanthan gum (XG). Formed suspension was mixed form 30 min at 300 rpm in darkness. The XG was used to avoid microcapsules aggregation.

Microcapsules characterization

Polyamide microcapsules mean size was determined using a HELOS BR supplied by Sympatec GmbH System Partikel Technik equipped with a R1 cuvette and a Helium-Neon Laser 5mW max output at 632.8 nm. The mean microcapsules size of the microcapsules was measured before and after 1 h of microcapsules irradiation with visible light emitted by a Philips DuraMax 85W 120V bulb. The analysis was carried out in xanthan gum and sodium sulfate water solution as a transport medium. Before analysis 0.1 g of microcapsules slurry was diluted with 50 mL solution containing 6 g sodium sulfate 0.35 g of xantham gum and 43.65 g demineralized water. Software setup and sample analysis were performed using Windox 5.8.0.0 software provided with the equipment by Sympatec. The sample analysis were performed in Free Mode, using Fraunhofer Enhanced Evaluation. The data were collected 2 times 5 s each.

Microcapsule morphologies were observed by using: Nikon optical microscopy equipped with bulb 12V DC (100W halogen lamp Philips 7724); Hitachi Model S-5200 scanning electron microscopy equipped with a Gatan Alto 2500 Cryotransfer System (Gatan Model CT2500) to cut the microcapsules. Atomic force microscopy studies were performed by a MultiMode AFM (Bruker, CA, USA) equipped with air probe holder (MMEFCH or similar) using Silicon AFM probes for imaging in air, OMCLAC160TS-W2 (Olympus, Japan) with the following nominal parameters: resonance frequency 300 kHz; spring constant 42 N/m; tip radius of curvature <10 nm, 7 nm. Before the AFM experiments, the microcapsules were deposited in darkness and dried on Si-wafers provided by Silicon Valley Microelectronics, CA, USA, with the following parameters: one-side highly polished, diameter: 200 mm, dopant: P/Boron, resistivity: 1–100 Ωcm, thickness: 725 μm, pre-cut to 12 mm×12 mm squares, with ~12 Å native oxide layer. Imaging was performed in tapping mode in air. The AFM red laser was illuminating the sample throughout its study. Scanning was performed in one direction – from top to bottom of slow scan axis. AFM data processing was performed using WSxM software, version 4.0 Develop 5.3 (Nanotec Electronica S.L., Spain). No tilt correction was applied to the images. Profile and Z-measurements on profiles were performed in reference to the same surface features in order to minimize thermal drift effects. A desk lamp equipped with a Philips DuraMax 85W 120V bulb served as the source of exposure for the microcapsules. The distance between the lamp and the sample was 30 cm. Light wavelenght emitted by this lamp (400–900 nm) was measured by an Ocean Optics USB2000 Miniature Fiber Optic Spectrometer, in a dark room at room temperature 23.0 ± 0.5 °C. Temperature of microcapsule surfaces, before and after exposure to light, was measured by an Omega MDSi8 thermometer (Omega Engineering) equipped with a thermocouple.

Acknowledgements: Financial support from European Community's Seventh Framework Programme (FP/2007–2013) under IOF Marie Curie grant agreement no. 328794, Horizon2020 ITN Marie Curie grant agreement no. 675624 and help of scientists from TPT P&G Cincinnati are gratefully acknowledged.

References

[1] J. Zhang, R. J. Coulston, S. T. Jones, J. Geng, O. A. Scherman, C. Abell. *Science* **335**, 690 (2012).
[2] V. Marturano, P. Cerruti, M. Giamberini, B. Tylkowski, V. Ambrogi. *Polymers* **9**, 8 (2017).

[3] J. Oh, B. Kim, S. Lee, S.-H. Kim, M. Seo. *Chem. Mater.* **30**, 273 (2018).
[4] R. E. Neisiany, J. K. Y. Lee, S. N. Khorasani, S. Ramakrishna. *Polym. Test.* **62**, 79 (2017).
[5] I. Nallamuthu, F. Khanum, S. J. Fathima, M. M. Patil, T. Anand. "Enhanced nutrient delivery through nanoencapsulation techniques: the current trend in food industry", in *Nutrient Delivery*, A. M. Grumezescu (Ed.), pp. 619–651, Academic Press, Cambridge, MA, USA (2017).
[6] J. Han, J. Bong, T. Lim, K.-H. Lee, H. Yang, S. Ju. *Appl. Surf. Sci.* **353**, 338 (2015).
[7] J. L. de Oliveira, E. V. R. Campos, M. Bakshi, P. C. Abhilash, L. F. Fraceto. *Biotechnol. Adv.* **32**, 1550 (2014).
[8] L. Paseta, E. Simón-Gaudó, F. Gracia-Gorría, J. Coronas. *Chem. Eng. J.* **292**, 28 (2016).
[9] J.-Z. Wang, Z.-Q. Ding, F. Zhang, W.-B. Ye. *Mater. Sci. Eng. C* **77**, 1247 (2017).
[10] M. Ghosh, S. Ghosh, M. Seibt, I. A. T. Schaap, C. F. Schmidt, G. Mohan Rao. *Appl. Surf. Sci.* **390**, 924 (2016).
[11] R. Saha, S. Verbanic, I. A. Chen. *Nat. Commun.* **9**, 2313 (2018).
[12] W. P. R. Deleu, G. Rivero, R. F. A. Teixeira, F. E. Du Prez, D. E. De Vos. *Chem. Mater.* **27**, 5495 (2015).
[13] S. Pan, J. Y. Ho, V. G. Chigrinov, H. S. Kwok. *ACS Appl. Mater. Interfaces* **10**, 9032 (2018).
[14] C. Hu, N. Ma, F. Li, Y. Fang, Y. Liu, L. Zhao, S. Qiao, X. Li, X. Jiang, T. Li, F. Shen, Y. Huang, Q. Luo, J. Liu. *ACS Appl. Mater. Interfaces* **10**, 4603 (2018).
[15] C. Hansell. *Nat. Chem.* **7**, 184 (2015).
[16] B. Tylkowski, A. Trojanowska, M. Giamberini, I. Tsibranska, M. Nowak, Ł. Marciniak, R. Jastrzab. *J. Membr. Sci. Res.* **3**, 265 (2017).
[17] A. P. Esser-Kahn, S. A. Odom, N. R. Sottos, S. R. White, J. S. Moore. *Macromolecules* **44**, 5539 (2011).
[18] J. Geng, W. Li, L. P. Smaga, N. R. Sottos, J. Chan. *Chem. Mater.* **30**, 2198 (2018).
[19] W. Guo, Y. Jia, K. Tian, Z. Xu, J. Jiao, R. Li, Y. Wu, L. Cao, H. Wang. *ACS Appl. Mater. Interfaces* **8**, 21046 (2016).
[20] A. A. Beharry, O. Sadovski, G. A. Woolley. *J. Am. Chem. Soc.* **133**, 19684 (2011).
[21] O. S. Bushuyev, M. Aizawa, A. Shishido, C. J. Barrett. *Macromol. Rapid Comm.* **39**, 1700253 (2018).
[22] B. Tylkowski, M. Giamberini, T. Underiner, S. F. Prieto, J. Smets. *Macromol. Symp.* **360**, 192 (2016).
[23] J. Borges, L. C. Rodrigues, R. L. Reis, J. F. Mano. *Adv. Funct. Mater.* **24**, 5624 (2014).
[24] G. G. D. Han, H. Li, J. C. Grossman. *Nat. Commun.* **8**, 1446 (2017).
[25] I. N. Lee, O. Dobre, D. Richards, C. Ballestrem, J. M. Curran, J. A. Hunt, S. M. Richardson, J. Swift, L. S. Wong. *ACS Appl. Mater. Interfaces* **10**, 7765 (2018).
[26] E. Mitscherlich. *Ann. Pharm.* **12**, 305 (1834).
[27] B. Tylkowski, A. Trojanowska, V. Marturano, M. Nowak, L. Marciniak, M. Giamberini, V. Ambrogi, P. Cerruti. *Coord. Chem. Rev.* **351**, 205 (2017).
[28] A. H. Gelebart, D. Liu, D. J. Mulder, K. H. J. Leunissen, J. van Gerven, A. P. H. J. Schenning, D. J. Broer. *Adv. Funct. Mater.* **28**, 10 (2018).
[29] M. Matsumoto, S. Terrettaz, H. Tachibana. *Adv. Colloid Interfac. Sci.* **87**, 147 (2000).
[30] F. Tanaka, T. Mochizuki, X. Liang, H. Asanuma, S. Tanaka, K. Suzuki, S.-I. Kitamura, A. Nishikawa, K. Ui-Tei, M. Hagiya. *Nano Lett.* **10**, 3560 (2010).
[31] P.-F. Cao, Z. Su, A. de Leon, R. C. Advincula. *ACS Macro Lett.* **4**, 58 (2015).
[32] X. Wang, Z. Li, Y. Yang, X. Gong, Y. Liao, X. Xie. *Langmuir* **31**, 5456 (2015).
[33] E. Blasco, B. V. K. J. Schmidt, C. Barner-Kowollik, M. Piñol, L. Oriol. *Macromolecules* **47**, 3693 (2014).
[34] A. Shulkin, H. D. H. Stöver. *Macromolecules* **36**, 9836 (2003).
[35] M. R. Molla, P. Rangadurai, L. Antony, S. Swaminathan, J. J. de Pablo, S. Thayumanavan. *Nat. Chem.* **10**, 659 (2018).
[36] M. Döbbelin, A. Ciesielski, S. Haar, S. Osella, M. Bruna, A. Minoia, L. Grisanti, T. Mosciatti, F. Richard, E. A. Prasetyanto, L. De Cola, V. Palermo, R. Mazzaro, V. Morandi, R. Lazzaroni, A. C. Ferrari, D. Beljonne, P. Samorì. *Nat. Commun.* **7**, 11090 (2016).
[37] M. J. Landry, M. B. Applegate, O. S. Bushuyev, F. G. Omenetto, D. L. Kaplan, M. Cronin-Golomb, C. J. Barrett. *Soft Matter* **13**, 2903 (2017).
[38] L. Cheng, Y. Jiang, S.-C. Qi, W. Liu, S.-F. Shan, P. Tan, X.-Q. Liu, L.-B. Sun. *Chem. Mater.* **30**, 3429 (2018).
[39] P. Bortolus, S. Monti. *J. Phys. Chem.* **83**, 648 (1979).
[40] P. Cattaneo, M. Persico. *Phys. Chem. Chem. Phys.* **1**, 4739 (1999).
[41] N. Kurita, S. Tanaka, S. Itoh. *J. Phys. Chem. A* **104**, 8114 (2000).
[42] A. Cembran, F. Bernardi, M. Garavelli, L. Gagliardi, G. Orlandi. *J. Am. Chem. Soc.* **126**, 3234 (2004).
[43] L. Gagliardi, G. Orlandi, F. Bernardi, A. Cembran, M. Garavelli. *Theor. Chem. Acc.* **111**, 363 (2004).
[44] L. Briquet, D. P. Vercauteren, J.-M. André, E. A. Perpète, D. Jacquemin. *Chem. Phys. Lett.* **435**, 257 (2007).
[45] J. Dokić, M. Gothe, J. Wirth, M. V. Peters, J. Schwarz, S. Hecht, P. Saalfrank. *J. Phys. Chem. A* **113**, 6763 (2009).
[46] D. Jacquemin, J. Preat, E. A. Perpète, D. P. Vercauteren, J.-M. André, I. Ciofini, C. Adamo. *Int. J. Quantum Chem.* **111**, 4224 (2011).
[47] J. Casellas, M. J. Bearpark, M. Reguero. *ChemPhysChem.* **17**, 3068 (2016).
[48] R. J. W. Le Fevre, J. Northcott. *J. Chem. Soc.* 867 (1953).
[49] P. H. Gore, O. H. Wheeler. *J. Org. Chem.* **26**, 3295 (1961).
[50] N. Norio, S. Toshinobu, Y. Hideyuki, I. Etsuko, Y. Shunzo, H. Shigeo. *Bull. Chem. Soc. Japan* **49**, 1381 (1976).
[51] S. Samanta, A. A. Beharry, O. Sadovski, T. M. McCormick, A. Babalhavaeji, V. Tropepe, G. A. Woolley. *J. Am. Chem. Soc.* **135**, 9777 (2013).

[52] Y. Yang, R. P. Hughes, I. Aprahamian. *J. Am. Chem. Soc.* **134**, 15221 (2012).
[53] D. Bléger, J. Schwarz, A. M. Brouwer, S. Hecht. *J. Am. Chem. Soc.* **134**, 20597 (2012).
[54] R. H. M. El Halabieh, O. Mermut, C. J. Barrett. *Pure Appl. Chem.* **76**, 1445 (2004).
[55] M. Irie, T. Suzuki. *Makromol. Chem.* **8**, 607 (1987).
[56] N. Biswas, S. Umapathy. *J. Phys. Chem. A* **101**, 5555 (1997).
[57] Q. Zhou, I. Fursule, B. J. Berron, M. J. Beck. *J. Phys. Chem. A* **120**, 7101 (2016).
[58] M. Staniszewska, S. Kupfer, M. Łabuda, J. Guthmuller. *J. Chem. Theory Comput.* **13**, 1263 (2017).
[59] S. Steinwand, T. Halbritter, D. Rastädter, J. M. Ortiz-Sánchez, I. Burghardt, A. Heckel, J. Wachtveitl. *Chem. Eur. J.* **21**, 15720 (2015).
[60] B. Tylkowski, M. Pregowska, E. Jamowska, R. Garcia-Valls, M. Giamberini. *Eur. Polym. J.* **45**, 1420 (2009).
[61] J. Smets. S. Fernandez Prieto; Smith, Steven Daryl; Underiner, Todd Laurence; Wos, John August; Huhn, Wolfgang Edgar; Frederick, Heath A.; Giamberini, Marta; Tylkowski, Bartosz. USA Patent 2013.
[62] T. Asano, T. Okada, S. Shinkai, K. Shigematsu, Y. Kusano, O. Manabe. *J. Am. Chem. Soc.* **103**, 5161 (1981).
[63] J. Dokić, M. Gothe, J. Wirth, M. V. Peters, J. Schwarz, S. Hecht, P. Saalfrank. *J. Phys. Chem. A* **113**, 6763 (2009).
[64] D. G. Whitten, P. D. Wildes, J. G. Pacifici, G. Irick. *J. Am. Chem. Soc.* **93**, 2004 (1971).
[65] K. Matczyszyn, W. Bartkowiak, J. Leszczynski. *J. Mol. Struct.* **565**, 53 (2001).
[66] M. Meilgaard, B. Carr, G. Civille, ed. *Sensory Evaluation Techniques*, CRC Press, Boca Raton (1999).
[67] E. J. Baerends, J. Autschbach, A. Bérces, C. Bo, P. M. Boerrigter, L. Cavallo, D. P. Chong, L. Deng, R. M. Dickson, D. E. Ellis, M. van Faassen, L. Fan, T. H. Fischer, C. F. Guerra, S. J. A. van Gisbergen, J. A. Groeneveld, O. V. Gritsenko, M. Grüning, F. E. Harris, P. v. d. Hoek, H. Jacobsen, L. Jensen, G. van Kessel, F. Kootstra, E. van Lenthe, D. A. McCormack, A. Michalak, V. P. Osinga, S. Patchkovskii, P. H. T. Philipsen, D. Post, C. C. Pye, W. Ravenek, P. Ros, P. R. T. Schipper, G. Schreckenbach, J. G. Snijders, M. Sola, M. Swart, D. Swerhone, G. te Velde, P. Vernooijs, L. Versluis, O. Visser, F. Wang, E. van Wezenbeek, G. Wiesenekker, S. K. Wolff, T. K. Woo, A. L. Yakovlev, T. Ziegler. (http://www.scm.com, accessed: 2014. *Scientific Computing and Modelling* ADF-2014.10).
[68] G. te Velde, F. M. Bickelhaupt, E. J. Baerends, C. Fonseca Guerra, S. J. A. van Gisbergen, J. G. Snijders, T. Ziegler. *J. Comput. Chem.* **22**, 931 (2001).
[69] A. D. Becke. *J. Chem. Phys.* **98**, 5648 (1993).
[70] C. Lee, W. Yang, R. G. Parr. *Phys. Rev. B* **37**, 785 (1988).
[71] E. Van Lenthe, E. J. Baerends. *J. Comput. Chem.* **24**, 1142 (2003).
[72] S. Hirata, M. Head-Gordon. *Chem. Phys. Lett.* **314**, 291 (1999).
[73] A. A. T. Clark, B. Beck, F. Burkhardt, J. Chandrasekhar, P. Gedeck, A. Horn, M. Hutter, B. Martin, G. Rauhut, W. Sauer, T. Schindler, T. Steinke. *Computer-ChemieCentrum*, Universität Erlangen-Nürnberg, Erlangen (2003).
[74] J. J. P. Stewart. *J. Mol. Model.* **10**, 155 (2004).